AD-A161 745 AIR MASS MODIFICATION IN THE MARGINAL ICE ZONE(U) 1/1
LAMONT-DOHERTY GEOLOGICAL OBSERVATORY PALISADES NY
T J BENNETT ET AL. NOV 85 LDGO-85-6 N00014-84-K-0735

UNCLASSIFIED F/G 4/1 NL

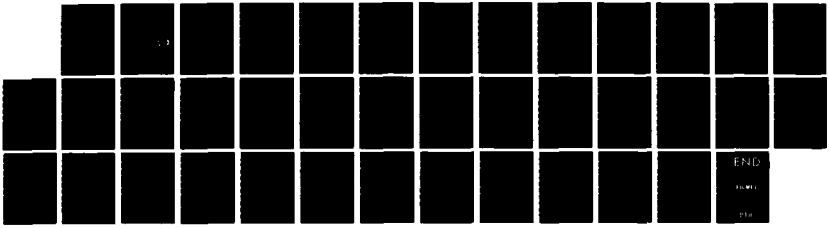

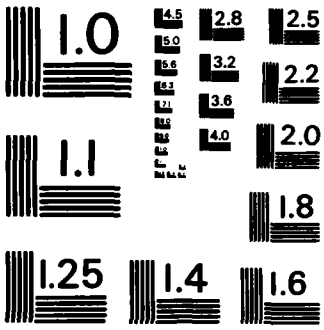

MICROCOPY RESOLUTION TEST CHART
NATIONAL BUREAU OF STANDARDS-1963-A

(2)

AD-A161 745

AIR MASS MODIFICATION IN THE MARGINAL ICE ZONE

Theodore J. Bennett, Jr.* and Kenneth Hunkins

FINAL TECHNICAL REPORT

LDGO-85-6

Contract N00014-84-K-0735

Department of the Navy
Office of Naval Research

DTIC
ELECTE
NOV 27 1985
S D
D

Lamont-Doherty Geological Observatory
of Columbia University
Palisades, New York 10964-0190

Approved for public release, distribution unlimited.

November 1985

* also at NASA Goddard Institute for Space Studies
2880 Broadway
New York, New York 10025

DTIC FILE COPY

85 11 27 004

TABLE of CONTENTS

Abstract.....iii

List of Figures.....iv

List of Tables.....v

Introduction.....1

Background.....2

Model Description.....4

Results.....8

Discussion.....12

References.....18

ABSTRACT

A case study of the Andreas et al. (1984) data on atmospheric boundary layer modification in the marginal ice zone is made. Our model is a two-dimensional, multi-level, linear model with turbulence, lateral and vertical advection, and radiation. Good agreement between observed and modeled temperature cross-sections is obtained. In contrast to the hypothesis of Andreas et al., we find the air flow is stable to secondary circulations. Cloud top longwave cooling, not an air-to-surface heat flux, dominates the cooling of the boundary layer. The accumulation with fetch over the ice of changes in the surface wind field are shown to have a large effect on estimates of the surface wind stress. We speculate that the Andreas et al. estimates of the drag coefficient over the compact sea ice are too high.

Keywords. Atmospheric boundary layers; Air-sea-ice interaction.

Accesion For
NTIS CRA&I ☑
DTIC TAB ☐
Unannounced ☐
Justification
By
Distribution /
Availability Codes
Dist | Avail and / or Special
A-1

QUALITY INSPECTED 3

LIST of FIGURES

Figure 1. A schematic diagram of a two-dimensional marginal ice zone. A model of the atmospheric boundary layer including simplified treatments of low level stratus clouds and sea ice thermodynamics is used to model the modification of the prescribed inflow. Modeled processes include turbulence, lateral and vertical advection and radiation. The bulk exchange coefficients for momentum, heat and moisture are functions of the ice concentration.

Figure 2a. A comparison of observed (from Andreas et al., 1984; solid) and modeled (dashed) ice edge wind profiles. The modeled profile is the prescribed inflow of the model (adapted from Andreas et al., 1984).

Figure 2b. A comparison of observed (from Andreas et al., 1984; solid) and modeled (dashed) ice edge potential temperature soundings. The modeled sounding is the prescribed inflow of the model (adapted from Andreas et al., 1984).

Figure 2c. The temperature, T, dew point, T_D, and liquid water mixing ratio, r_ℓ, soundings used to prescribe the model inflow.

Figure 3. Potential temperature soundings at the ice edge and at fetches of 40, 80, 120 and 150 km for the rough simulation.

Figure 4. A height-fetch cross-section of potential temperature (°C; above) and the initial fraction of open water (below) for the rough simulation. The stippled regions in the upper figure indicate liquid water mixing ratios greater than 0.01 g/kg.

Figure 5. The heat budget for the rate of change of potential temperature of the air column at a fetch of 150 km in the rough simulation. The corresponding potential temperature sounding is shown in Figure 3. Processes include turbulence, total radiation (longwave plus shortwave) and vertical and lateral advection.

Figure 6. The 25 m drag coefficients, C_D, and bulk exchange coefficients for sensible heat, C_H, for the rough (solid), smooth (dashed), and intermediate (dotted) simulations. In the intermediate simulation $C_H = C_D$.

Figure 7. The 25 m surface wind speed, ν, and surface wind stress, τ, of the rough (solid), smooth (dashed), and intermediate (dotted) simulations.

Figure 8. Same as Figure 4 but for the intermediate surface simulation.

LIST of TABLES

Table 1 A test of the stability to secondary circulations forced by inflection point instability of the atmospheric boundary layer at several points downwind of the ice edge and several possible angles ε between the axis of the secondary roll and the geostrophic wind. The height of the inflection point, Z_{INF}, of the cross-roll velocity profile; the local Richardson number, Ri_{ℓ}, at the inflection point; and the height of the inversion are given for the rough simulation. Secondary circulations are unlikely when $Ri_{\ell} > 0.25$.

Table 2 Drag coefficients (10^3 C_D) referred to 10 m anemometer level over small, rafted floes of concentrations 0.8 - 0.9 (from Overland, 1985).

Introduction

The marginal ice zone (MIZ) is a boundary zone between the polar and temperate parts of the climate system (Untersteiner et al., 1983; Johannessen et al., 1983). An important aspect of the MIZ of the Bering and Weddell Seas is the intense rate of destruction of sea ice that had formed in the coastal polynyas and then drifted with little change in thickness toward the open ocean (Pease, 1980; Hibler and Ackley, 1983). What MIZ processes are responsible for this destruction and how is it coupled to the ocean and atmosphere?

Andreas et al. (1984) have made a data study of the modification of the atmospheric boundary layer in the MIZ. During an episode of on-ice winds in the Weddell Sea, they obtained wind and temperature soundings at the ice edge and four additional temperature soundings along a 150 km, along-wind track into the ice cover. In their analysis, they have suggested that the destruction of sea ice in the MIZ is episodic. In particular, they have suggested that during episodes of strong on-ice winds, there is a large air-to-surface heat flux, perhaps due to secondary flows, which could result in rapid ice ablation.

A two-dimensional model of the atmospheric boundary layer based on the Herman and Goody (1976) arctic stratus cloud model, together with simple sea ice and oceanic mixed layer thermodynamics, is used to make a case study of the Andreas et al. (1984) data. We use their ice edge wind and temperature soundings as a prescribed inflow and calculate the modification of the atmospheric boundary layer as it flows on-ice. A model simulation which incorporates the exchange coefficients appropriate for a rough broken ice cover

(Andreas et al., 1984) is used to test several results and hypotheses of the Andreas et al. (1984) analysis. This model simulation is also compared to a simulation which uses prescribed, open ocean exchange coefficients in order to obtain an estimate of the effect of incorporating realistic surface roughness on calculations of the surface wind stress and heat flux. These simulations are referred to as the "rough" and "smooth" simulations, respectively.

Background

The Andreas et al. (1984) data study has several specific results and hypotheses that can be readily tested with our model. The principal results and hypotheses include:

a) observed soundings and height-fetch cross-sections of potential temperature that can be compared with model results;

b) there is a large air-to-surface heat flux over the rough, MIZ ice cover, perhaps due to secondary flow, which results in large rates of ice ablation;

c) the rise with fetch of the isentropes above the inversion base is the result of adiabatic lifting due to upward motion forced by low-level convergence.

One goal of the Andreas et al. (1984) study was to measure the drag coefficient over the MIZ ice. Overland (1985) has recently reviewed a number of field measurements of the drag coefficient over sea ice. In his review, he emphasizes the dependence of the drag coefficient on form drag, the upwind surface roughness, the height of the atmospheric inversion and the atmospheric

stability. The relationship between the drag coefficients and the exchange coefficients for heat and moisture has been discussed by Walter et al. (1984).

An important aspect of this study is the modification of the air flow over a change in surface roughness. Much of the earlier field work on this topic is limited to very shallow layers and short fetches. These studies include Bradley (1968); the Risö studies (Petersen et al., 1980 and references cited therein), and Ogawa and Ohara (1985). The Andreas et al. (1984) study is the first MIZ-scale study of on-ice air flow. Off-ice flow has been examined by Overland et al. (1983) and Reynolds (1984), while the analogous passage of cold air over the Great Lakes has been considered by Lenschow (1973) and Stage and Businger (1981). Other relevant studies are Rao et al. (1974) and Taylor (1971), who have done some modeling, and Hogström and Smedman-Hogström (1985), who have discussed some data and modeling work. Additional data and modeling work is being done in association with MIZEX, the Marginal Ice Zone Experiment (see Johannessen et al., 1983).

Among published models of the atmospheric boundary layer applicable to the MIZ, the one most relevant to our study is the one used at the Pacific Marine Environmental Laboratory (Overland et al., 1983; Reynolds, 1984). It is a one layer model and is used to model off-ice air flow. The one layer approximation is useful during off-ice situations because strong surface heating of the cold air over the relatively warm water leads to convection and a uniform sounding of equivalent potential temperature. However, the situation observed by Andreas et al. (1984) is stably stratified. Our approach to determining the turbulent fluxes and stability to secondary flow is to make multi-layer calculations of the wind shear and temperature lapse rate.

Recently, Davidson et al. (1984) have used a single layer model of the marine atmospheric boundary layer which permits a constant vetical gradient in the mixed layer properties. These models are thus distinctive in their approach or applicability.

Model Description

A multi-level, linear, Boussinesq model of the atmospheric boundary layer which closely follows the model of Herman and Goody (1976) is used. The principal variables are θ_E, the equivalent potential temperature; r, the total water mixing ratio (the sum of the water vapor and liquid water mixing ratios); and the wind velocity components of u, in the on-ice, x direction; v in the cross-ice, y direction; and w, in the upward direction. This atmosphere is described by

$$\frac{\partial \Theta_E}{\partial t} = -(U_o + u)\frac{\partial \Theta_E}{\partial x} - w\frac{\partial \Theta_E}{\partial z} - \frac{\partial}{\partial z}\left(K\frac{\partial \Theta_E}{\partial z}\right) + Q_{RAD}\left(\frac{\Theta_E}{T}\right) \qquad (1)$$

$$\frac{\partial r}{\partial t} = -(U_o + u)\frac{\partial r}{\partial x} - w\frac{\partial r}{\partial z} - w_F\frac{\partial r_L}{\partial z} - \frac{\partial}{\partial z}\left(K\frac{\partial r}{\partial z}\right) \qquad (2)$$

$$\frac{\partial u}{\partial t} = -U_o\frac{\partial u}{\partial x} + fv - \frac{\partial}{\partial z}\left(K\frac{\partial u}{\partial z}\right) - \frac{1}{\rho_o}\frac{\partial p}{\partial x} \qquad (3)$$

$$\frac{\partial v}{\partial t} = -U_o\frac{\partial v}{\partial x} - fu - \frac{\partial}{\partial z}\left(K\frac{\partial v}{\partial z}\right) \qquad (4)$$

$$\frac{\partial w}{\partial z} = -\frac{\partial u}{\partial x} \qquad (5)$$

Other variables include K, the vertical eddy diffusivity; Q_{RAD}, the radiative heating term; r_L, the liquid water mixing ratio; and f, the Coriolis parameter. These equations have been linearized about a base state, on-ice wind U_o of 13 m s^{-1}.

A number of processes are included. The calculation of Q_{RAD} and K and the specification of w_F, the drop fall speed, and other drop variables follow Herman and Goody (1976). Using a single, constant drop size in the radiation scheme is a potentially serious limitation (Tsay, Jayaweera and Stamnes, 1983), but we believe the model is still useful in identifying the basic physics of atmospheric boundary layer modification in the MIZ. In these calculations, we assume we are in the northern hemisphere and the date is April 21. Pressure p is calculated by the Boussinesq approximation (Schatzmann and Policastro, 1984).

The boundary conditions are chosen so that we can make a case study of the Andreas et al. (1984) data. Figure 1 is a schematic diagram of the situation. The wind and potential temperature profiles of the inflow are prescribed using several linear segments to approximate the ice edge data of Andreas et al. (1984). They did not have any useful data on the moisture profile. We have, therefore, examined the Arctic stratus cloud data of Tsay and Jayaweera (1984) and have rather arbitrarily prescribed a "reasonable" inflow moisture profile. Modeled and observed inflow profiles are compared in Fig. 2. Note the wind shear minimum between 400-500 m. We will consider it below. The atmosphere above 2 km is prescribed from the 60°N July U.S. Standard Atmosphere (Dubin et al., 1966). We have chosen to prescribe the turbulent fluxes at the top of the model domain (2 km) rather than prescribe

Θ_E and r or use a zero flux condition because these fluxes are more consistent with the observed wind shear and vertical gradient of potential temperature near 2 km. These fluxes are -0.018 deg. m s^{-1} and -6.8 x 10^{-7} m^2 s^{-1}, respectively. A positive flux is upward. The initial ice concentrations are based on the observations of Andreas et al. (1984).

Bulk aerodynamic formulas are used to calculate the surface turbulent fluxes of sensible heat, moisture and momentum. The open ocean, 25 m drag coefficient is set to equal to 1.07 x 10^{-3}. It is obtained by assuming neutral stability, a constant momentum flux between 10 m and 25 m and a 10 m drag coefficient of 1.25 x 10^{-3} (from Fig. 17.2 of Charnock (1981) with a 10 m wind of 7.5 m s^{-1}). In the "smooth" simulation, we use the open ocean drag coefficient at all grid points. In the "rough" simulation, we accept the Andreas et al. (1984) estimate of how the drag coefficient varied with fetch. Using their Eqn. 4, we set the ratio of the drag coefficient over ice of concentration C, $C_D(C)$, to the open ocean value, C_D^o, to be

$$\frac{C_D(C)}{C_D^o} = 1 + 2.4 \tanh (2.5\ C) \quad .$$

The applicability of their Eqn. 14 is discussed below. The exchange coefficient for heat, C_H, was not estimated by Andreas et al. (1984). In a study over the Bering Sea, Walter et al. (1984) measured the ratio C_H/C_D to be 0.20 - 0.28 over rough sea ice which had a drag coefficient of $C_D = 3.0 \pm 0.6 \times 10^{-3}$. They noted that their measurement of C_H/C_D was consistent with earlier results that C_H/C_D is 1.1 over a smooth surface but decreases rapidly as the surface roughness increases beyond a certain critical value. The peak Andreas

et al. (1984) estimate of $C_D = 4.0 \times 10^{-3}$ is larger than the C_D measured by Walter et al. (1984) and suggests that C_H/C_D ought to be small in our case study. Hence, we set $C_H/C_D = 1.1$ in the "smooth" simulation and in the "rough" simulation, which has a wide range of ice concentration, $C_H/C_D = 1-C$. The latter relationship is ad hoc but incorporates the gross dependence of C_H/C_D on surface roughness. The exchange coefficient for moisture, C_E is set equal to C_H (Walter et al., 1984).

The surface incorporates a simple formulation of sea ice thermodynamics (ablation) based on the 0 - layer model of Semtner (1976) and a heat budget calculation of lateral ice ablation. For simplicity, the sea ice has no snow cover. There is only one mixed layer temperature in a grid length and it can not exceed the freezing point of sea water if sea ice exists. A 50 m deep, motionless oceanic mixed layer is used; salinity is not considered. Further development of the mixed layer part of the model is planned.

It is a two-dimensional model with forty 50 m deep layers in the vertical and seventeen 10 km long intervals in the horizontal, perpendicular to the ice edge direction. Radiative heating and convective adjustment are calculated once every 12 mintues. At time intervals of 2 minutes, a smoother with $s_1 = 0.5$ and $s_2 = -0.5$ is applied to each vertical profile of Θ_E (Haltiner, 1971, pp. 270-274). The use of a smoother is necessary in order to remove some ripple-like features from the simulations. An Euler forward time step is used with the radiative. Upwind differences are used to calculate the lateral and vertical advection terms. Time-stepping of these and the other terms in Eqns. (1) to (4) use Method A of Young (1968) with a time step of 40 s. This is also the time increment for the surface heat budget and ice ablation calcula-

tions. Although these time steps were satisfactory for a number of runs, the rough simulation required a time step of 13.3 s with Method A.

Results

The vertical soundings and fetch-height sections of potential temperature of the rough simulation, Figs. 3 and 4, respectively, generally agree well with the observations of Andreas et al. (1984), their Figs. 2 and 6, respectively. We find the base of the inversion rises from a height of 525 m at the ice edge to about 875-900 m at a fetch of 150 km. It also crosses isentropes from its initial potential temperature of 4°C to a final value of about 6.5-7.0°C. Andreas et al. (1984) observed the outflowing inversion base to be at a height of 1050 m and a potential temperature of 6.4°C. The top of the inversion is smoothed out in the model simulations. The modeled contours of potential temperature within and above the inversion rise with fetch although the modeled cooling is smaller than observed. Below a height of 500 m, there is a small warming with increasing fetch in the model atmosphere but a cooling of perhaps 1C in the observations. The gross features of the modeled cloud, shown by the stippling in Fig. 4, agree with the observations of Tsay and Jayaweera (1984). These features include a cloud top at the base of the inversion and at longer fetches the occurrence of the largest liquid water mixing ratios near the top of the cloud.

Although this model is not capable of simulating secondary flows, we hope to be able to say whether they are likely to exist. Our approach is to associate the model wind and temperature profiles with the mean flow on to which the horizontal vortex rolls of the secondary flow are added and test

whether this mean flow is stable to secondary circulations. There are two major energy sources for rolls -- convective and dynamic instabilities (Brown, 1980). Theoretically, these sources can act independently. However, Müller et al. (1985) have noted that the rolls are generally observed in situations with unstable stratification and these two sources usually can not be distinguished. They have suggested that inflection point instability acts as a trigger for roll development which is enhanced by buoyancy if there is unstable stratification.

If the atmosphere were dry, it would be stably stratified since $\Theta_z > 0$. The subscript z indicates $\frac{\partial}{\partial z}$. The moisture profiles must be considered before we can say whether the soundings of equivalent potential temperature are stable. We can say, however, that if the 500-m thick layer between the heights of 375 m and 875 m were to have $(\Theta_E)_z = 0$, then the water vapor mixing ratio, r_v, would have to decrease by approximately 1.3 g/kg over that depth. In the model, however, r_v becomes increasingly uniform below the inversion base as the fetch increases. Since the air is warmer than the surface in the model and they are approximately the same in the observations, we expect little buoyancy to be generated at the surface. We conclude that convection is unlikely.

Following Brown (1980), we test for dynamic instabilities. The Reynolds number Re is on the order of 600 or larger, which is in the inflection point instability regime (LeMone, 1973). We consider a longitudinal roll axis at an angle ε to the geostrophic wind and the wind profile in a plane prependicular to the roll. If the local Richardson number

$$Re_{\ell} = \left(\frac{g}{\overline{T}}\right)\left(\frac{T_z + g/c_p}{u_z^2}\right)$$

at the inflection point is greater than 0.25, then the inflection point instabilities are suppressed. In the above, g is the acceleration of gravity, and $\overline{T}$ is a mean temperature. Applying this test to the rough simulation gives the results shown in Table 1. The local Richardson number, Ri_{ℓ}, is much greater than 0.25 at all angles ε and fetches. The flow is, however, less stable with increasing fetch because of a steepening of the wind shear. We conclude that secondary flows, are unlikely to occur during the period of the Andreas et al. (1984) observations.

Above the inversion base, the rise of the isentropes with fetch is the result of vertical advection. The dominant terms in the heat budget at these heights are the cooling due to vertical advection and the warming due to lateral advection (see Fig. 5). In the reference frame of an air parcel flowing downstream, lateral advection is zero and vertical advection dominates. The modeled vertical velocity is 1 - 3 cm s^{-1}, which agrees well with the Andreas et al. (1984) estimate of 2 cm s^{-1}. The model processes forcing the upward motion are a slowing of the zonal wind because of a Coriolis-forced turning to the right, which has a maximum at a height of about 0.5 km and at fetches greater than 80 km, and a low-level convergence forced by surface friction.

The heat budget for the rate of change of potential temperature of the air column at a fetch of 150 km in the rough simulation is shown in Fig. 5. The corresponding potential temperature sounding is shown in Fig. 3. The turbulent flux is downward at all levels but a minimum wind shear at 800 m causes a flux minimum at that level and the turbulent warming near 875 m.

Below the height of the minimum flux, turbulence acts to make the vertical gradient of potential temperature uniform. This region is the planetary boundary layer and it is capped by the inversion. Above the wind shear minimum, the wind fields of the rough and smooth simulation are the same. Strong longwave cooling is associated with the cloud top at 950 m. Cooling due to adiabatic lifting is also strong near and above the cloud top.

The cloud top/inversion base rises to a greater height in the rough simulation than in the smooth simulation. The effect of turbulence generated by surface friction extends to a greater height over the rougher surface. Hence, the height of the wind shear minimum and the depth of the boundary layer increase.

The effect of incorporating a realistically rough surface into calculations of the surface wind stress can be estimated by comparing the rough and smooth simulations. The 25 m bulk exchange coefficient for heat and momentum of the two simulations are compared in Fig. 6. In the rough simulation, the decrease in the 25 m wind speed across the model domain (Fig. 7) agrees well with the observed decrease in 21 m wind speed from 10 m s^{-1} at the inflow to 8.0 m s^{-1} at the outflow. When the drag coefficient is fetch dependent, the maximum wind stress does not necessarily occur at the point of maximum wind speed or maximum drag coefficient. In the rough simulation, the maximum wind stress occurs upstream of the maximum drag coefficient because of the cumulative slowing of the wind across the domain. The cumulative slowing of the wind is much smaller in the smooth simulation. The domain-averaged wind stress is 0.208 J m^{-3} in the rough simulation and 0.129 J m^{-3} in the smooth simulation. The rough/smooth ratio of the domain-averaged wind stresses

(1.61) is reduced by the relatively small wind stresses at fetches greater than 110 km despite the large drag coefficients. These results are relevant to the problem of estimating MIZ-scale ice drift.

There are similar effects on the surface turbulent heat flux. The downward sensible heat flux in the lowest several hundred meters is larger in the rough simulation because of the larger wind shear. At long fetches, the surface heat flux decreases because of the smaller bulk exchange coefficients and slower wind speeds of the rough simulation. As a result, the temperature of the lower boundary layer and, hence, the air-surface temperature difference increases. This warming is not found in the observations, which limits the relevance of our heat flux calculations to estimating what would be observed. However, we can note that maximum surface heat flux occurs near the middle of the domain. Comparing the surface wind speed, bulk exchange coefficient and air-surface temperature difference, we find the surface heat flux at a fetch of 130 km is smaller in the rough simulation because of the slower wind speed. These results indicate that quantitative estimates of the surface turbulent flux of sensible heat and momentum must incorporate not only an appropriately rough exchange coefficient but the effect of the surface roughness on the surface wind and air-surface temperature difference as well.

Discussion

Our model estimates of the surface turbulent flux of sensible heat are an order of magnitude less than the estimates made by Andreas et al. (1984) using the integral method. The dominant term in the cooling of the model boundary layer is the longwave cooling at the cloud top and we believe it is the major

part of the heat loss between the soundings used in their method. Apparently, Andreas et al. (1984) did not consider this term and instead attributed its effect to a surface flux of sensible heat. Cloud top long wave cooling has an important role in the theory and modeling of cloud topped planetary boundary layers. It has been discussed, for example, by Herman and Goody (1976), who used a model upon which ours is based, Lilly (1968), and Nieuwstadt and Businger (1984).

We doubt the Andreas et al. (1984) equation relating ice concentration and drag coefficient is generally applicable. As we noted above, the drag coefficient is a function of form drag (Arya, 1973; 1975), the upwind surface roughness (Macklin, 1983), the height of the atmospheric inversion and the atmospheric stability (Overland, 1985). In order to estimate the drag coefficient in MIZ modeling studies, a composite table of drag coefficients for various ice regimes, air temperatures and other variables, such as that compiled by Overland (1985, Table 6), would perhaps be more appropriate.

How reasonable are the drag coefficients estimated by Andreas et al. (1984)? We suggest that the drag coefficients are actually smaller than their estimates.

Although a number of field measurements have shown that the MIZ C_D can be substantially larger than the open ocean C_D, the Andreas et al. (1984) estimate of $C_D = 4.0 \times 10^{-3}$ over ice of concentration 0.8 is larger than any of the drag coefficients included in the composite table compiled by Overland (1985, Table 6). The ice regime of small rafted ice floes with a concentration of 0.8 - 0.9, characteristic of the inner MIZ, has among the highest C_D given in his table. These coefficients are repeated in our Table 2. The ob-

served meteorological regime is $T_a \sim 0°C$ and $Z_i > 400$ m, where T_a is the air temperture and Z_i is the inversion height. The larger coefficients in Table 2 are for $T_a < -5$ C. In this situation, the open leads and thin ice areas are a source of buoyancy, which increases C_D (Overland, 1985). Since $T_a \sim 0$ in the Andreas et al. (1984) data, we expect little or no buoyancy to be generated in these areas. In addition, stable stratification, which is characteristic of these data, is associated with smaller drag coefficients. Inspecting composite table of C_D found in Overland (1985, Table 6), one might speculate that C_D should be in the range of $2.2 - 2.6 \times 10^{-3}$.

The sensitivity of the model simulation to the values of the bulk exchange coefficients is tested by making an "intermediate" surface simulation and comparing it to the other cases. Since we speculate that the Andreas et al. (1984) estimates of C_D are too high, we multiply the (25 m) ratio $C_D(C)/C_D^o$ by a factor of 0.67. In order to increase the surface heat flux, we set $C_H = C_E = C_D$. The 25 m C_D is shown in Fig. 6. The surface wind speed and wind stress are similar to those of the rough simulation (Fig. 7). There is again good agreement between the observed and modeled dependence of wind speed on fetch. A height-fetch section of potential temperature (Fig. 8) shows that the potential temperature of the lowest 500 m at long fetches agrees better with the observations than the rough simulation does but the 1°C contour still does not appear. In fact, the 1°C contour does not appear even if we use C_D of the rough simulation and set $C_H = C_D$. As expected, the adiabatic lifting of the isentropes above the inversion and the rise of the inversion with fetch are smaller in the intermediate simulation than in the rough simulation.

Acknowledgment

This research was supported by the Office of Naval Research under contract N00014-84-K-0735. This is Lamont-Doherty Geological Observatory contribution LDGO-85-6.

TABLE 1

Stability to Secondary Circulations Forced by Inflection Point Instability.
Secondary Circulations are Suppressed when $Ri_\ell = \gtrsim 0.25$.

	40 km Downwind (Z_i = 475 m)			80 km Downwind (Z_i = 625 m)			150 km Downwind (Z_i = 875 m)		
	$\varepsilon = 10°$	$\varepsilon = 0°$	$\varepsilon = -10°$	$\varepsilon = 10°$	$\varepsilon = 0°$	$\varepsilon = -10°$	$\varepsilon = 10°$	$\varepsilon = 0°$	$\varepsilon = -10°$
Z_{INF}	175 m	325 m	475 m	225 m	325 m	425 m	275 m	375 m	475 m
Ri_ℓ	5.58	22.9	85.6	5.06	13.5	35.9	3.37	7.00	14.4

Z_{INF} = height of inflection point, Ri_ℓ = local Richardson number, Z_i = height of inversion

TABLE 2

Drag Coefficients (10^3 C_D) Referred to 10 m Anemometer Level Over Small, Rafted Floes of Concentrations 0.8 - 0.9 (from Overland, 1985).

$T_a \sim 0C$	$T_a < -5C$ $Z_i < 300$ m	$T_a < -5C$ $Z_i > 400$ m
2.6	3.0	3.7

T_a = air temperature, Z_i = inversion height

References

Andreas, E.L., W.B. Tucker, III, and S.F. Ackley, Atmospheric boundary-layer modification, drag coefficient, and surface heat flux in the Antarctic marginal ice zone, J. Geophys. Res., 89, 649-661, 1984.

Arya, S.P.S., Contribution of form drag on pressure ridges to the air stress on Arctic ice, J. Geophys. Res., 78, 7092-7099, 1973.

Arya, S.P.S., A drag partition theory for determing the large-scale roughness parameter and wind stress on the Arctic pack ice, J. Geophys. Res., 80, 3447-3454, 1975.

Bradley, E.F., A micrometeorological study of velocity profiles and surface drag in the region modified by a change in roughness, Q.J.R. Meteorol. Soc., 94, 361-379, 1968.

Brown, R.A., Longitudinal instabilities and secondary flows in the planetary boundary layer: A review, Rev. Geophys. Space Phys., 18, 683-697, 1980.

Charnock, H., Air-sea interaction, in Evolution of Physical Oceanography, ed. by Warren and Wunsch, MIT Press, pp. 482-503, 1981.

Davidson, K.L., C.W. Fairall, P.J. Boyle, and G.E. Schacher, Verification of an atmospheric mixed-layer model for a coastal region, J. Climate Appl. Meteorol., 23, 617-636, 1984.

Dubin, M., N. Sissenwine, and S. Teweles, (Co-Chairmen), U.S. Standard Atmosphere Supplements, 1966, p. 145, U.S. Government Printing Office, 1966.

Haltiner, G.J., Numerical Weather Prediction, John Wiley and Sons, pp. 270-274, 1971.

Herman, G.F., and R. Goody, Formation and persistence of summertime Arctic stratus clouds, J. Atmos. Sci., 33, 1537-1553, 1976.

Hibler, W.D., III, and S.F. Ackley, Numerical simulation of the Weddell Sea pack ice, J. Geophys. Res., 88, 2873-2887, 1983.

Hibler, W.D., III, and K. Bryan, Ocean circulation: its effects on seasonal sea-ice simulations, Science, 224, 489-492, 1984.

Hogstrom, U., and A.-S. Smedman-Hogstrom, The wind regime in coastal areas with special reference to results obtained from Swedish wind energy program, Boundary Layer Meteorol., 30, 351-373, 1984.

Johannessen, O.M., W.D. Hibler, III, P. Wadhams, W.J. Campbell, K. Hasselmann, I. Dyer, M. Dunbar, MIZEX: A Program for Mesoscale Air-Ice-Ocean Interaction Experiments in Arctic Marginal Ice Zones II. A Science Plan for a Summer Marginal Ice Zone Experiment in the Fram Strait/Greenland Sea: 1984, CRREL Special Report 83-12, 1983.

LeMone, M.A., The structure and dynamics of horizontal roll vortices in the planetary boundary layer, J. Atmos. Sci., 30, 1077-1091, 1973.

Lenschow, D.H., Two examples of planetary boundary layer modification over the Great Lakes, J. Atmos. Sci., 30, 568-581, 1973.

Macklin, S.A., Wind drag coefficient over first-year sea ice in the Bering Sea, J. Geophys. Res., 88, 2845-2852, 1983.

Muller, D., D. Etling, Ch. Kottmeier, and R. Roth, On the occurrence of cloud streets over northern Germany, Q.J.R. Metoerol. Soc., III, 761-772, 1985.

Ogawa, Y., and T. Ohara, The turbulent structure of the internal boundary layer near the shore, Boundary Layer Meteorol., 31, 369-384, 1985.

Overland, J.E., R.M. Reynolds, and C.H. Pease, A model of the atmospheric boundary layer over the marginal ice zone, J. Geophys. Res., 88, 2836-2840, 1983.

Pease, C.H., Eastern Bering Sea ice processes, Mon. Wea. Rev., 108, 2015-2023, 1980.

Peterson, E.W., P.A. Taylor, J. Jojstrup, N.O. Jensen, L. Kristensen, and E.L. Petersen, Riso 1978: Further investigations into the effects of local terrain irregularities on tower-measured wind profiles, Boundary Layer Meteorol., 19, 303-313, 1980.

Rao, K.S., J.C. Ayngaard, and O.R. Cote, The structure of the two-dimensional internal boundary layer over a sudden change of surface roughness, J. Atmos. Sci., 31, 738-746, 1974.

Reynolds, R.M., On the local meteorology at the marginal ice zone of the Bering Sea, J. Geophys. Res., 89, 6515-6524, 1984.

Schatzmann, M., and A.J. Policastro, Effects of the Boussinesq approximation on the results of strongly-buoyant plume calculations, J. Climate Appl. Meteorol., 23, 117-123, 1984.

Semtner, A.J., Jr., A model for the thermodynamic growth of sea ice in numerical investigations of climate, J. Phys. Oceanogr., 379-389, 1976.

Stage, S.A., and J.A. Businger, A model for entrainment into a cloud-topped marine boundary layer. Part I: model description and application to a cold-air outbreak episode, J. Atmos. Sci., 38, 2213-2229, 1981.

Taylor, P.A., Airflow above changes in surface heat-flux, temperature and roughness: an extension to include the stable case, Boundary Layer Meteorol., 1, 474-479, 1971.

Tsay, S.-C., and K. Jayaweera, Physical characteristics of Arctic stratus clouds, J. Climate Appl. Meteorol., 23, 584-596, 1984.

Untersteiner, N. (ed.), Air-Sea-Ice. Research Program for the 1980s Scientific Plan, 83 pp., Univ. of Washington, 1983.

Walter, B.A., J.E. Overland, and R.O. Gilmer, Air-ice drag coefficients for first-year sea ice derived from aircraft measurements, J. Geophys. Res., 89, 3550-3560, 1984.

Young, J.A., Comparative properties of some time differencing schemes for linear and nonlinear oscillations, Mon. Wea. Rev., 96, 357-364, 1968.

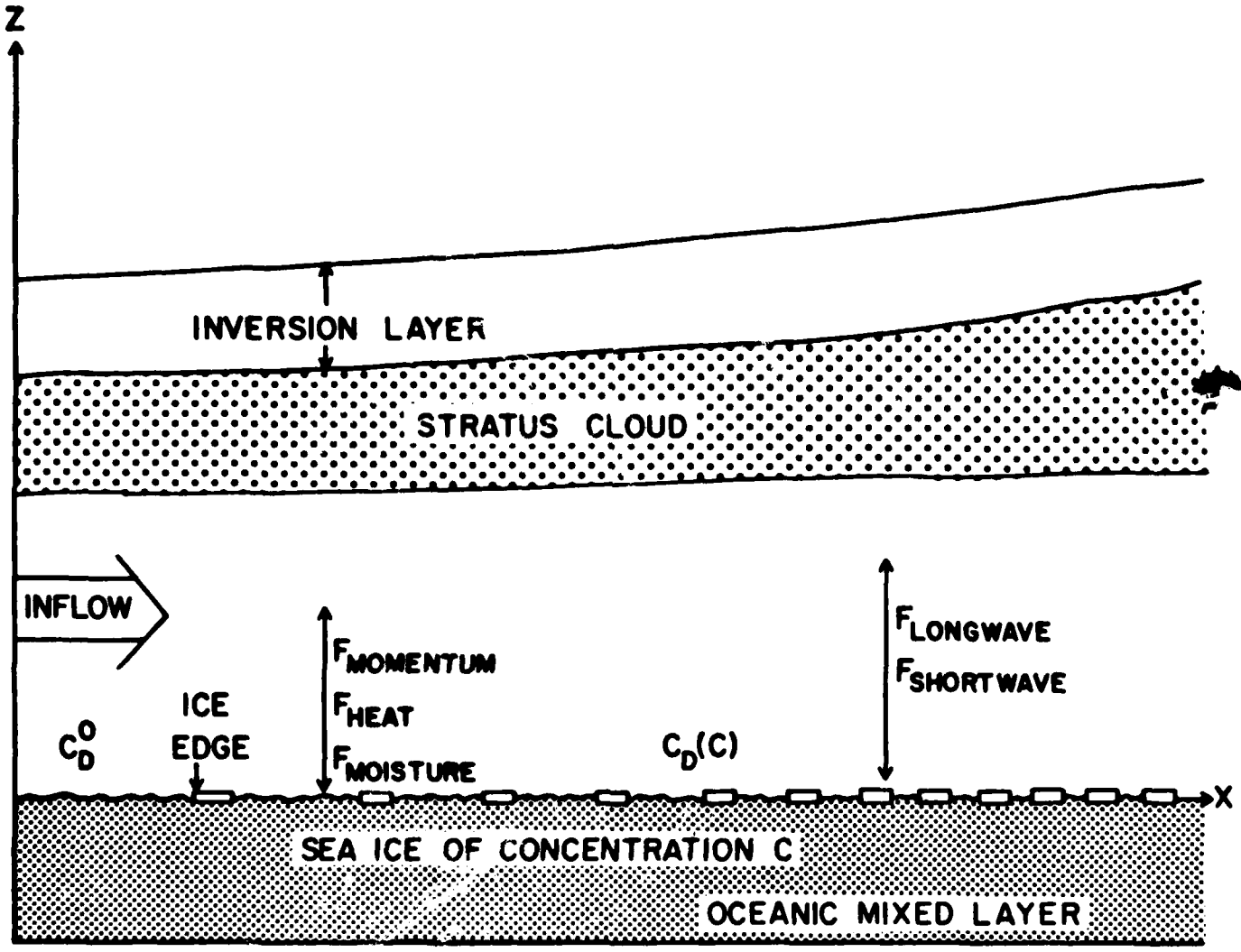
Z
INVERSION LAYER
STRATUS CLOUD
INFLOW
C_D^O
ICE
EDGE
$F_{MOMENTUM}$
F_{HEAT}
$F_{MOISTURE}$
$C_D(C)$
$F_{LONGWAVE}$
$F_{SHORTWAVE}$
X
SEA ICE OF CONCENTRATION C
OCEANIC MIXED LAYER

Figure 1

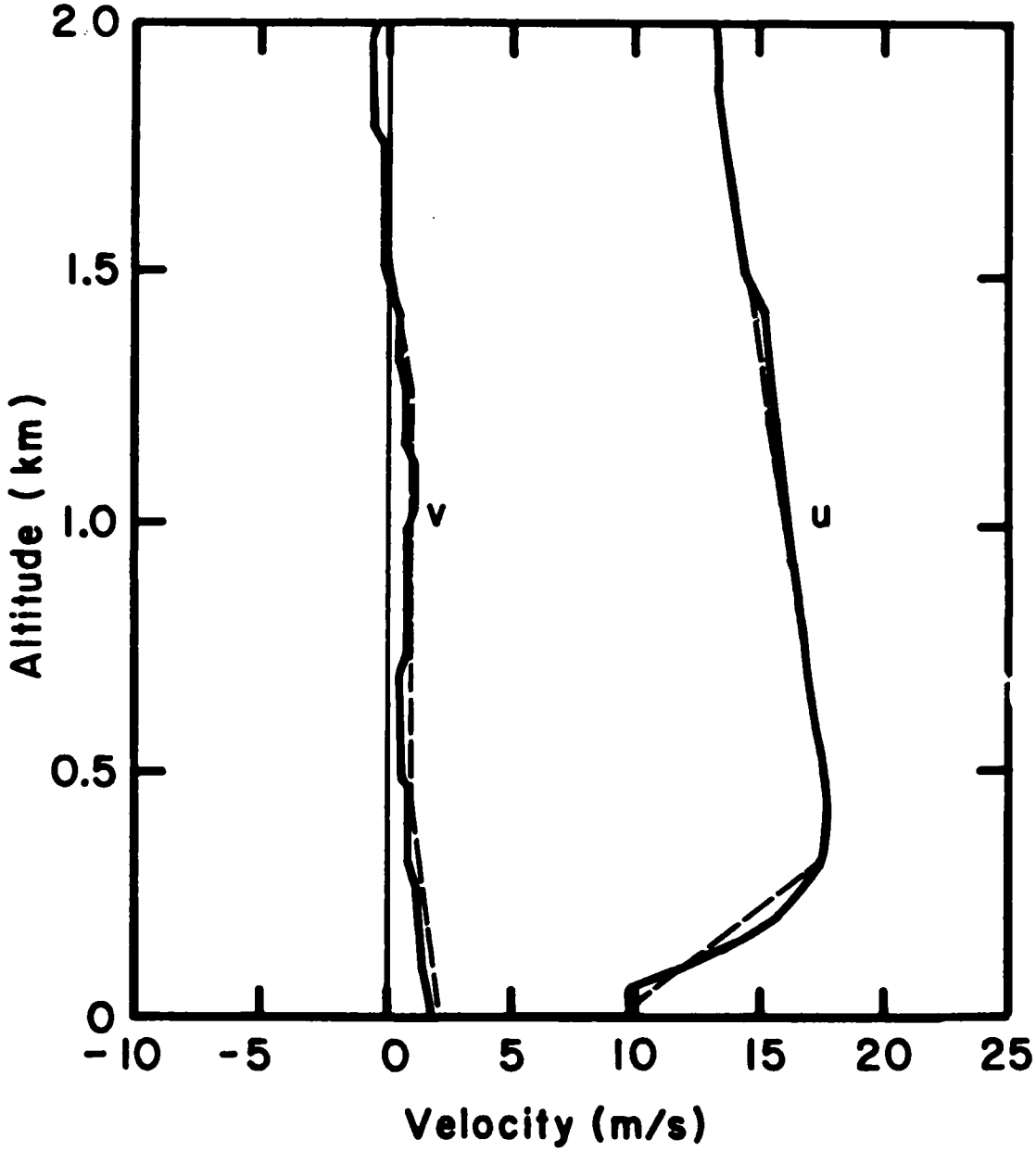

Figure 2a

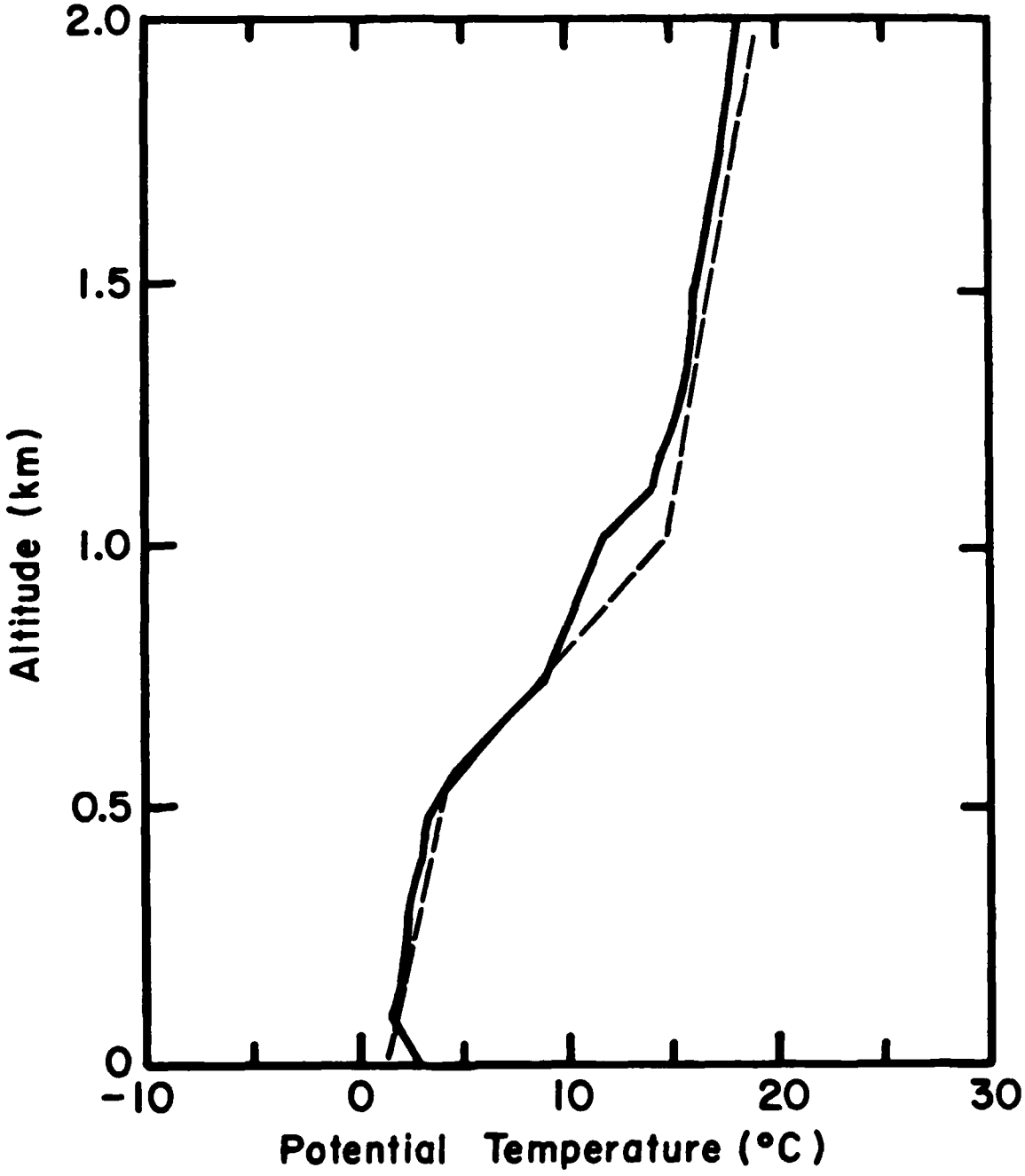

Figure 2b

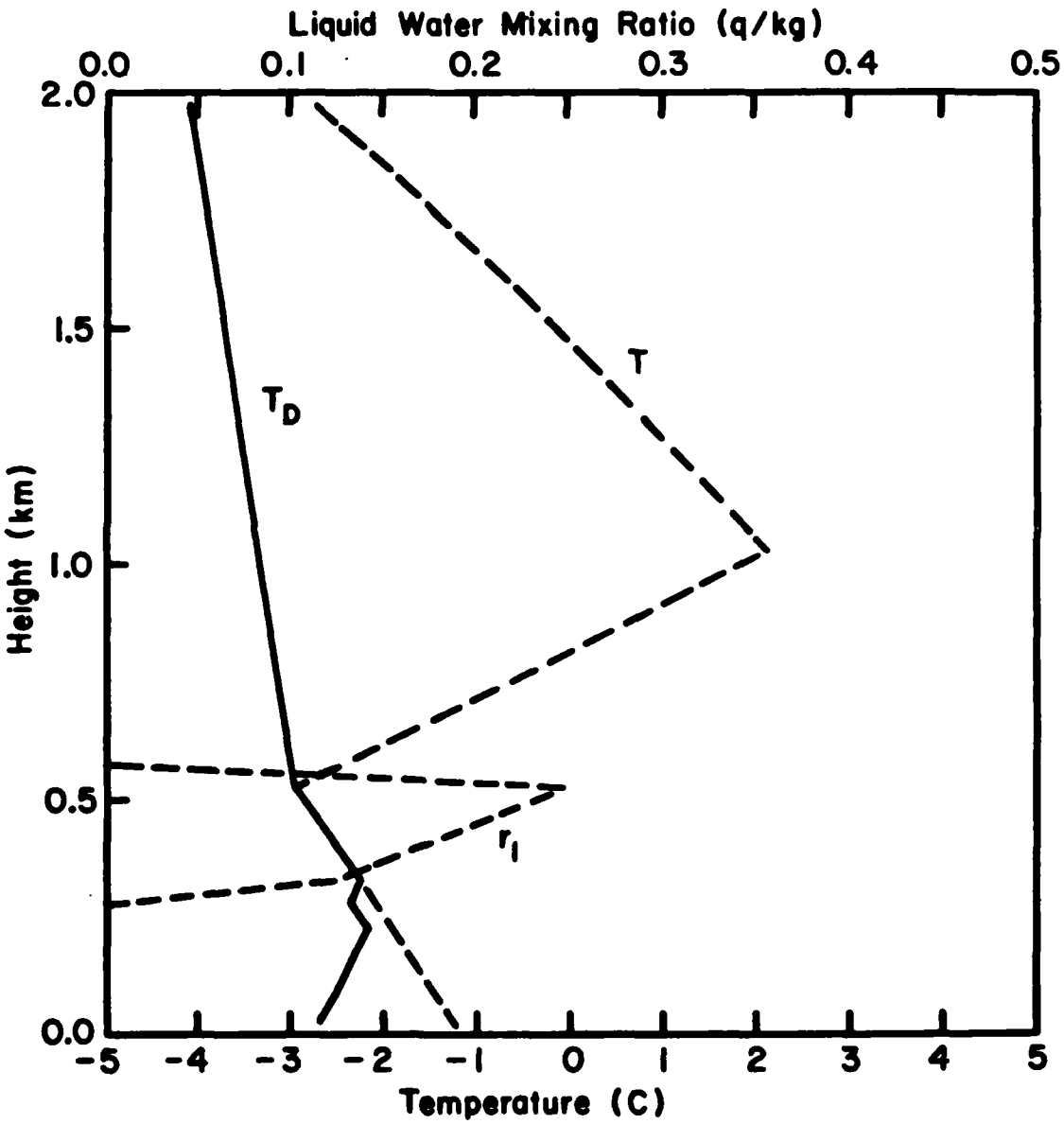
Liquid Water Mixing Ratio (q/kg)
0.0
0.1
0.2
0.3
0.4
0.5
2.0
1.5
1.0
0.5
0.0
Height (km)
T
T_D
r_l
-5
-4
-3
-2
-1
0
1
2
3
4
5
Temperature (C)

Figure 2c

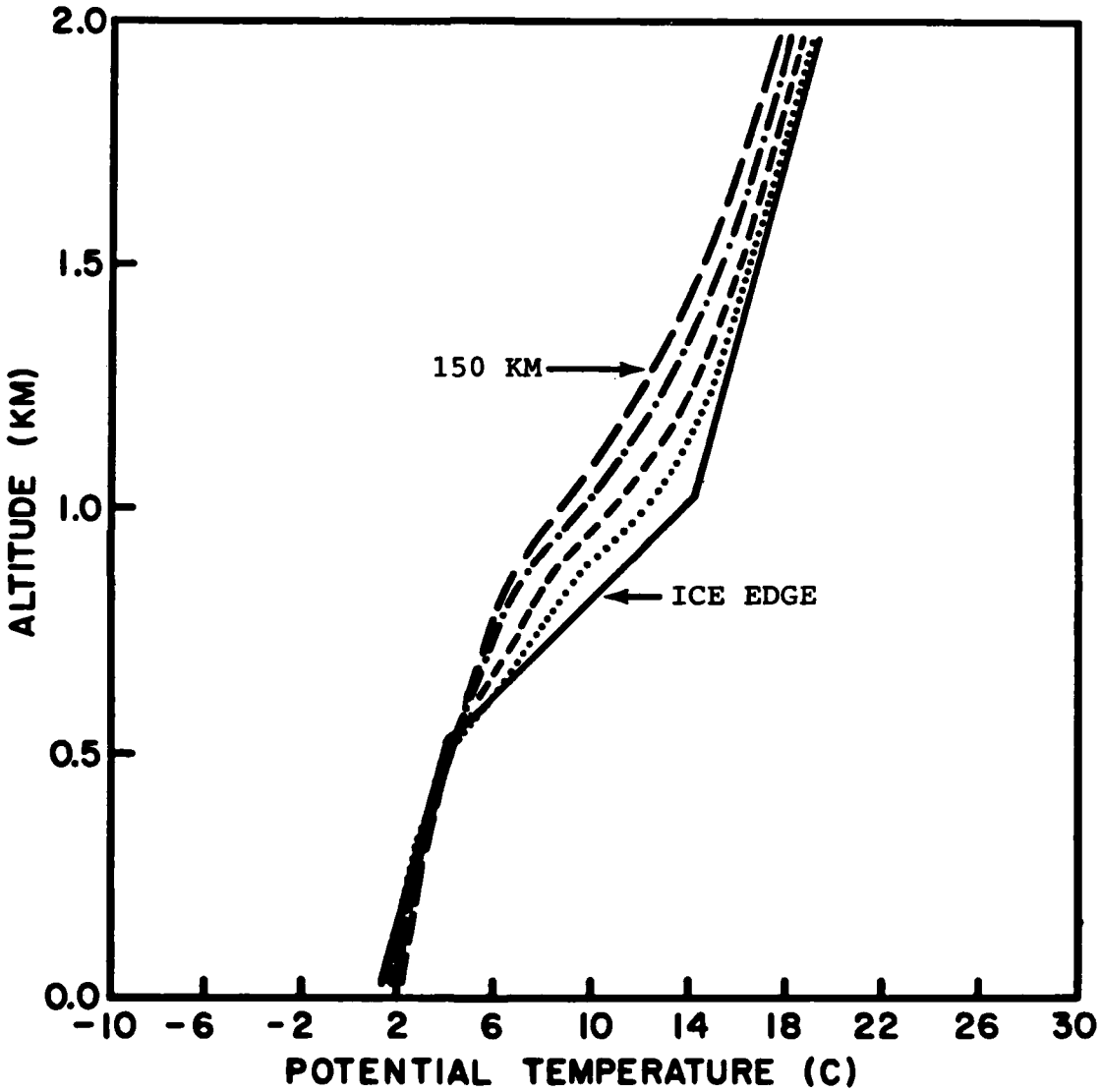
2.0
1.5
1.0
0.5
0.0
ALTITUDE (KM)
150 KM
ICE EDGE
-10
-6
-2
2
6
10
14
18
22
26
30
POTENTIAL TEMPERATURE (C)

Figure 3

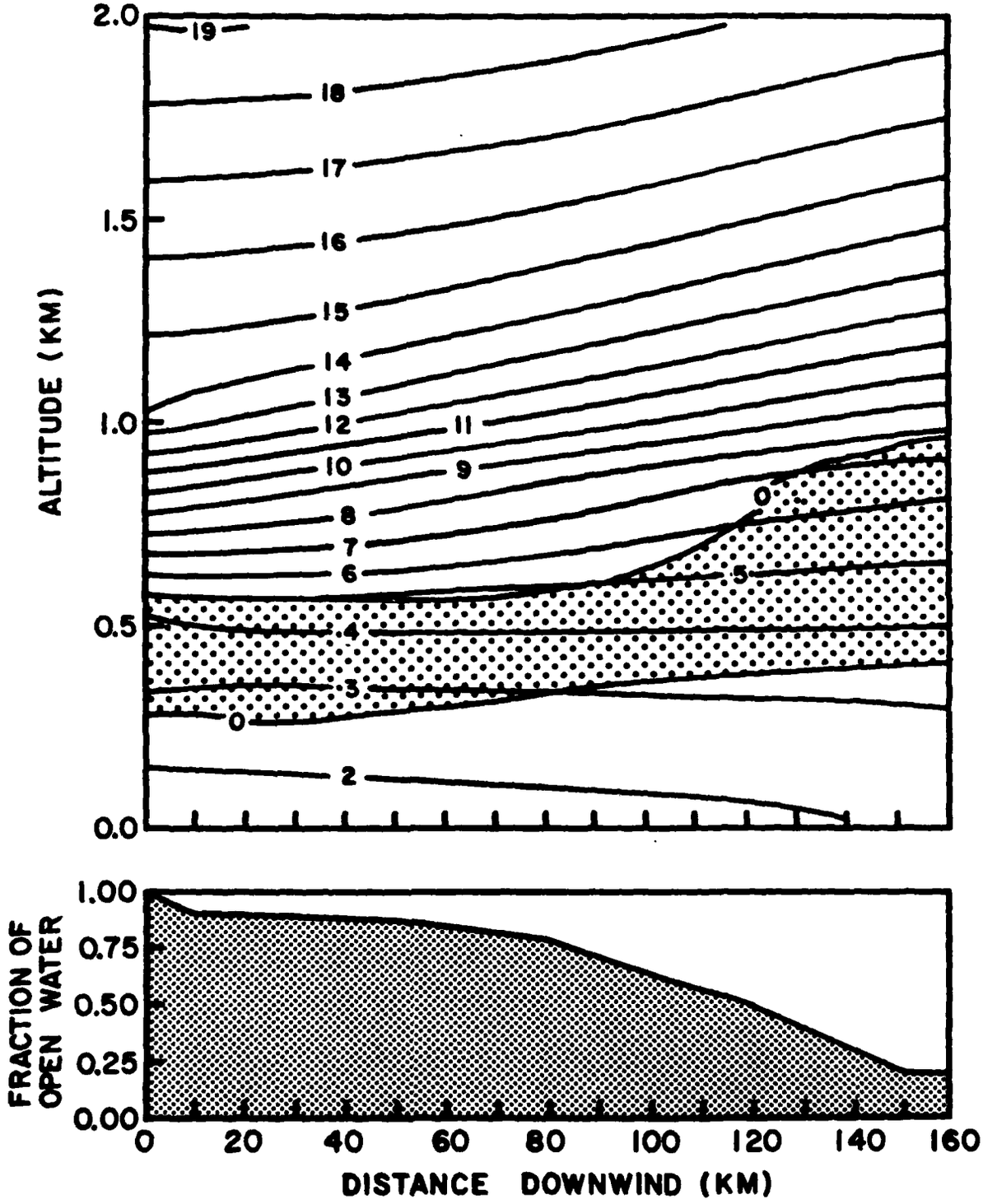
2.0
1.5
1.0
0.5
0.0
ALTITUDE (KM)
19
18
17
16
15
14
13
12
11
10
9
8
7
6
5
4
3
2
0
1.00
0.75
0.50
0.25
0.00
FRACTION OF OPEN WATER
0
20
40
60
80
100
120
140
160
DISTANCE DOWNWIND (KM)

Figure 4

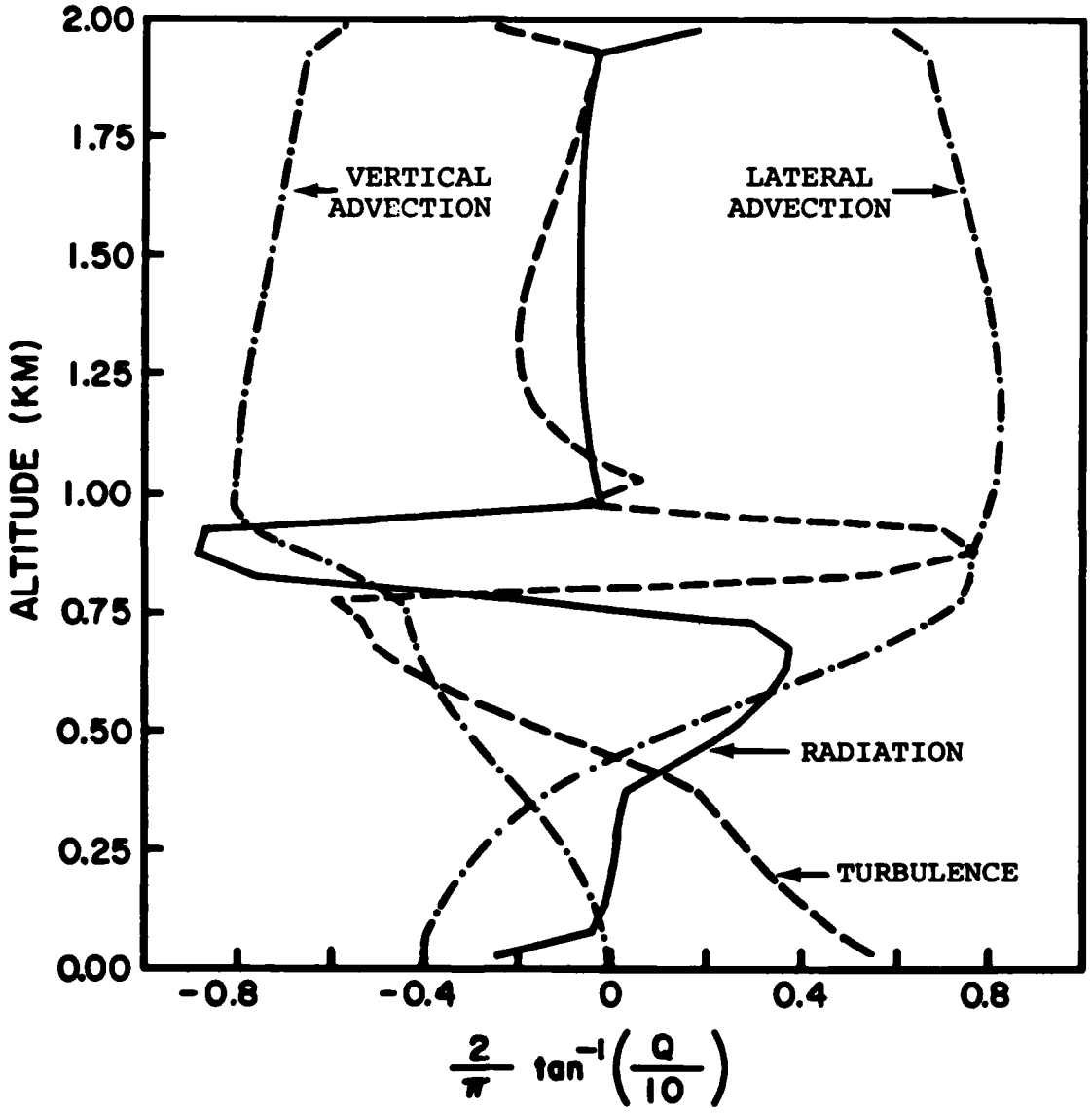
2.00
1.75
1.50
1.25
1.00
0.75
0.50
0.25
0.00
ALTITUDE (KM)
VERTICAL ADVECTION
LATERAL ADVECTION
RADIATION
TURBULENCE
-0.8
-0.4
0
0.4
0.8
$\frac{2}{\pi} \tan^{-1}\left(\frac{Q}{10}\right)$

Figure 5

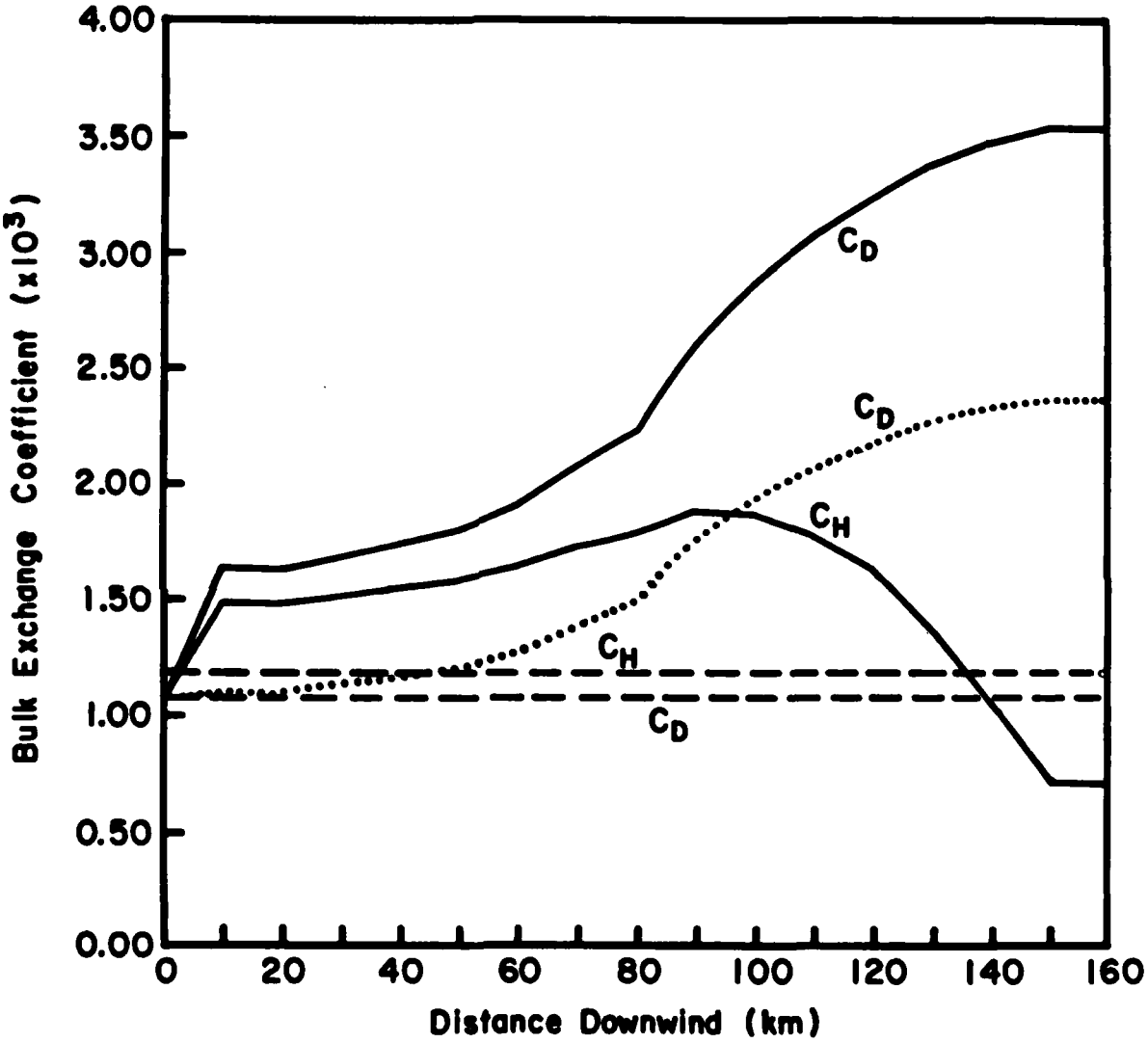
4.00
3.50
3.00
2.50
2.00
1.50
1.00
0.50
0.00
Bulk Exchange Coefficient (x10³)
0
20
40
60
80
100
120
140
160
Distance Downwind (km)
C_D
C_D
C_H
C_H
C_D

Figure 6

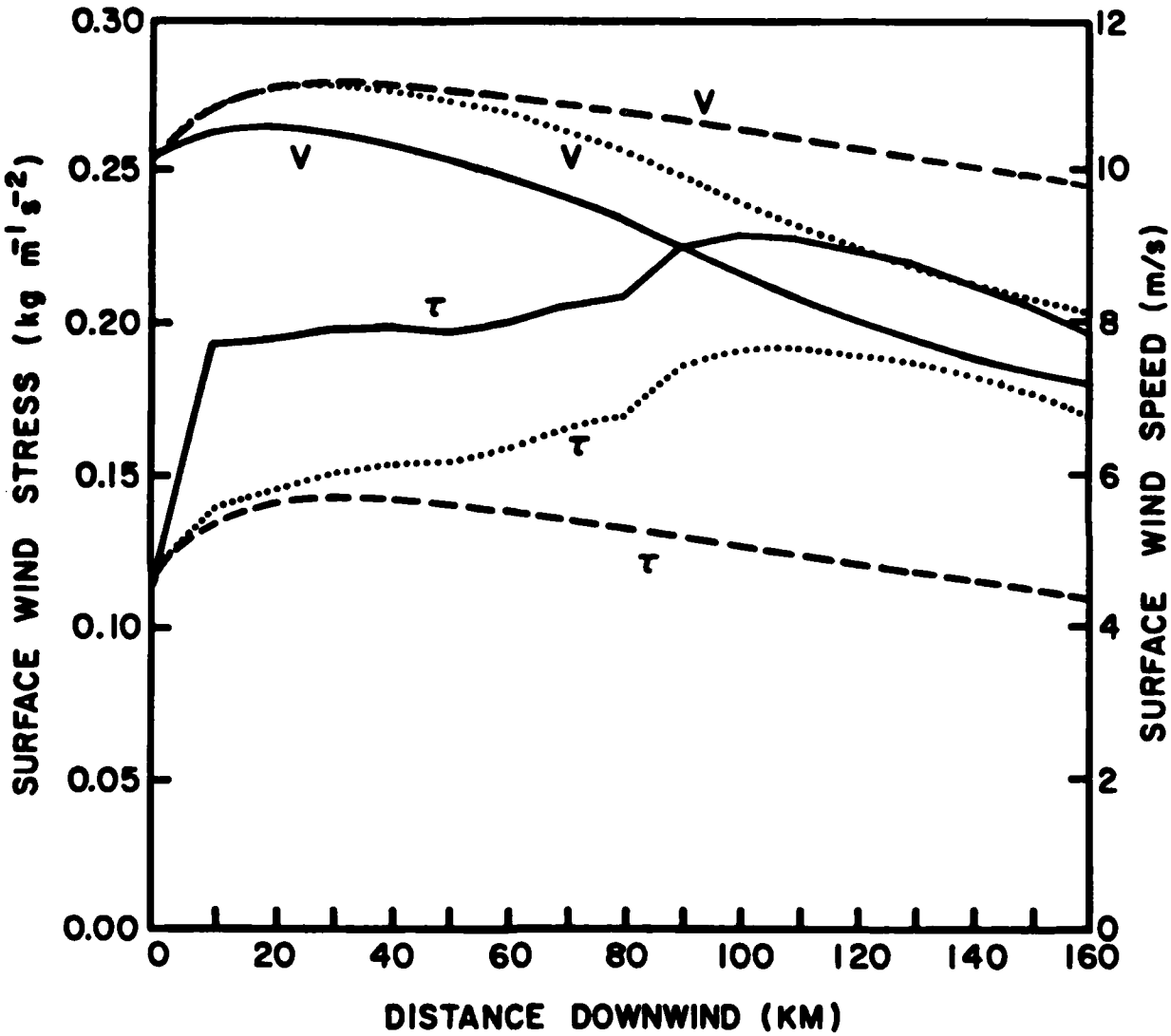
0.30
0.25
0.20
0.15
0.10
0.05
0.00
SURFACE WIND STRESS (kg m⁻¹ s⁻²)
12
10
8
6
4
2
0
SURFACE WIND SPEED (m/s)
0
20
40
60
80
100
120
140
160
DISTANCE DOWNWIND (KM)
V
V
V
τ
τ
τ

Figure 7

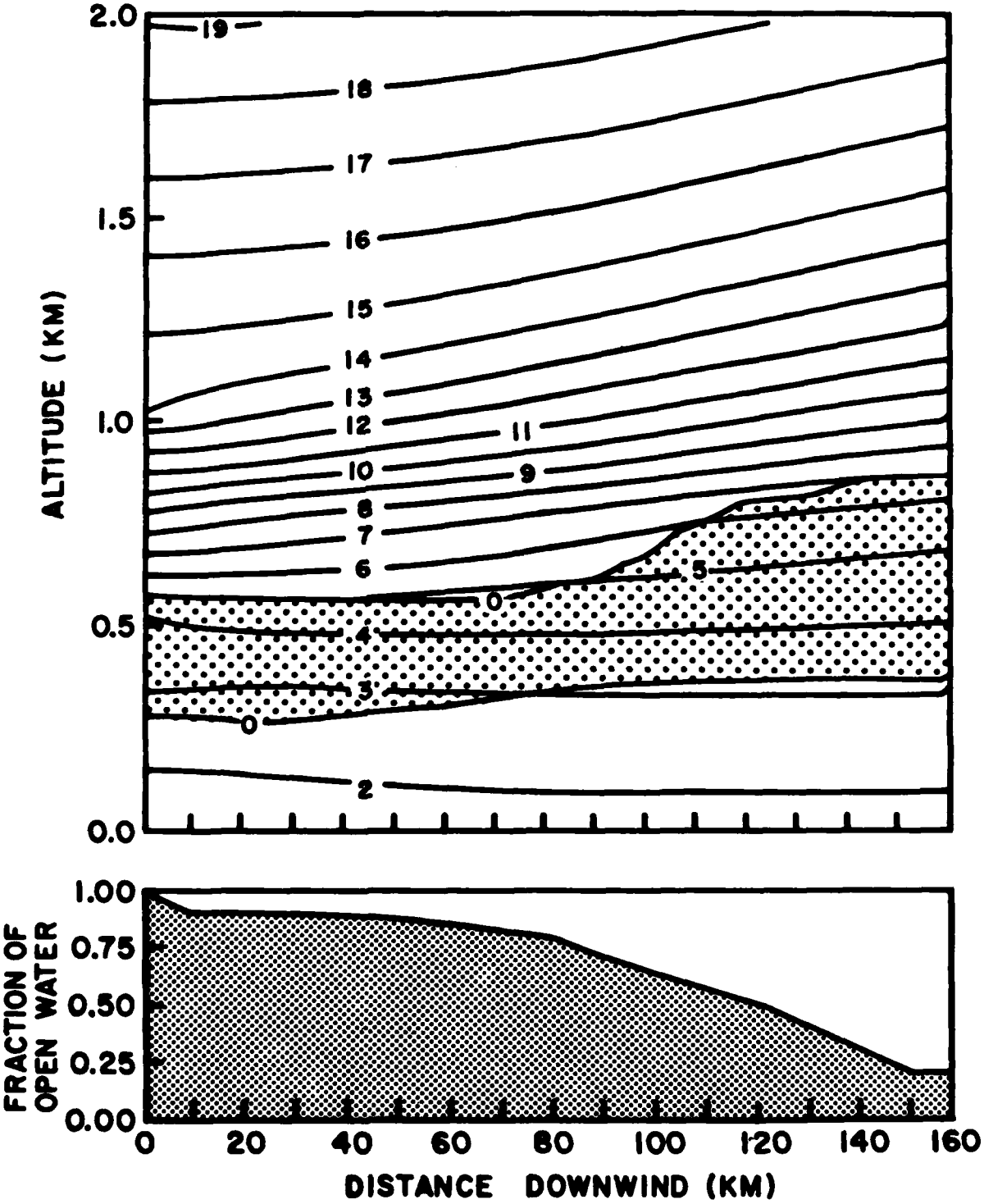
2.0
1.5
1.0
0.5
0.0
ALTITUDE (KM)
19
18
17
16
15
14
13
12
11
10
9
8
7
6
5
0
4
3
0
2
1.00
0.75
0.50
0.25
0.00
FRACTION OF OPEN WATER
0
20
40
60
80
100
120
140
160
DISTANCE DOWNWIND (KM)

Figure 8

MANDATORY DISTRIBUTION LIST

Dr. G. Leonard Johnson Arctic Sciences, Code 1125AR Office of Naval Research 800 N. Quincy Street, BCT No. 1 Arlington, VA 22217-5000	1
Mr. Gus Bellisari Office of Naval Research 715 Broadway, 5th Floor New York, NY 10003	*
Naval Research Laboratory Washington, DC 20375 DODAAD Code N 00173	1
Defense Documentation Center Building 5 Cameron Station Alexandria, VA 22314	2

UNCLASSIFIED

SECURITY CLASSIFICATION OF THIS PAGE (When Data Entered)

REPORT DOCUMENTATION PAGE

READ INSTRUCTIONS BEFORE COMPLETING FORM

1. REPORT NUMBER: LDGO-85-6	2. GOVT ACCESSION NO.: AD-A161745
3. RECIPIENT'S CATALOG NUMBER:	
4. TITLE (and Subtitle): AIR MASS MODIFICATION IN THE MARGINAL ICE ZONE	5. TYPE OF REPORT & PERIOD COVERED: Final Technical Report
	6. PERFORMING ORG. REPORT NUMBER:
7. AUTHOR(s): Theodore J. Bennett, Jr. and Kenneth Hunkins	8. CONTRACT OR GRANT NUMBER(s): N00014-84-K-0735
9. PERFORMING ORGANIZATION NAME AND ADDRESS: Lamont-Doherty Geological Observatory of Columbia University Palisades, New York 10964-0190	10. PROGRAM ELEMENT, PROJECT, TASK AREA & WORK UNIT NUMBERS:
11. CONTROLLING OFFICE NAME AND ADDRESS: Office of Naval Research Arctic Sciences, Code 1125AR Arlington, Virginia 22217-5000	12. REPORT DATE: November 1985
	13. NUMBER OF PAGES: 35
14. MONITORING AGENCY NAME & ADDRESS (if different from Controlling Office):	15. SECURITY CLASS. (of this report): Unclassified
	15a. DECLASSIFICATION/DOWNGRADING SCHEDULE:

16. DISTRIBUTION STATEMENT (of this Report)

Approved for public release, distribution unlimited.

17. DISTRIBUTION STATEMENT (of the abstract entered in Block 20, if different from Report)

18. SUPPLEMENTARY NOTES

19. KEY WORDS (Continue on reverse side if necessary and identify by block number)

Atmospheric boundary layers
Air-sea-ice interaction
Sea ice

20. ABSTRACT (Continue on reverse side if necessary and identify by block number)

A case study of the Andreas et al. (1984) data on atmospheric boundary layer modification in the marginal ice zone is made. Our model is a two-dimensional, multi-level, linear model with turbulence, lateral and vertical advection, and radiation. Good agreement between observed and modeled temperature cross-sections is obtained. In contrast to the hypothesis of Andreas et al., we find the air flow is stable to secondary circulations.

DD FORM 1 JAN 73 1473 EDITION OF 1 NOV 65 IS OBSOLETE
S/N 0102-LF-014-6601

UNCLASSIFIED

SECURITY CLASSIFICATION OF THIS PAGE (When Data Entered)

Cloud top longwave cooling, not an air-to-surface heat flux, dominates the cooling of the boundary layer. The accumulation with fetch over the ice of changes in the surface wind field are shown to have a large effect on estimates of the surface wind stress. We speculate that the Andreas et al. estimates of the drag coefficient over the compact sea ice are too high.

END

FILMED

1-86

DTIC